Ridge-Shaped Narrow Wall Directional Coupler Using TE_{10}, TE_{20}, and TE_{30} Modes

TOSHIAKI TANAKA

Abstract—**A new type of compact narrow wall directional coupler, whose coupling region is a ridge waveguide having dimensions such that TE_{10}, TE_{20}, and TE_{30} modes can exist, is proposed and analyzed. Coupling ratio and nonreflecting condition are determined by the degree of interference between TE_{20} and TE_{30} modes, and between TE_{10} and TE_{30} modes, respectively. The coupler can be used as a variable power divider by varying the coupling slot height. For 3-dB coupling over the 16.0 to 19.0-GHz frequency range, power equality within ±0.5 dB, more than 30-dB isolation and more than 30-dB return loss can be obtained. Experimental coupling results have shown good agreement with the theory.**

I. Introduction

A WAVEGUIDE directional coupler plays an important part in microwave circuits. Short-slot coupler [1] and Transvar coupler [2] have been well known as a tight-coupling narrow wall directional coupler. Ideally in these couplers, the output wave phase of the auxiliary guide lags that of the main guide by 90°. The short-slot coupler consists of a suitably loaded gap in the common narrow wall between two waveguides and matching elements. The Transvar coupler consists of a long coupling slot containing a grid of wires in the common narrow wall of the two waveguides. The coupling region of the above two couplers is an oversized waveguide, having dimensions such that only TE_{10} (symmetrical) and TE_{20} (antisymmetrical) modes can exist and TE_{30} mode is beyond cutoff. The fundamental operation of these couplers can be described by mutual interference between TE_{10} and TE_{20} modes [3].

On the other hand, the operation principle of the ridge-shaped directional coupler presented here is based on the mutual interference among TE_{10}, TE_{20}, and TE_{30} modes in the coupling region. Therefore, this coupler has the following features:

(1) the structure is very simple and no matching element is needed;

(2) a number of coupling waveguides geometrical arrangements are possible;

(3) the auxiliary guide output signal leads the main branch signal by 90°;

(4) it operates as a variable power divider by varying the coupling slot height.

Manuscript received August 28, 1979; revised October 18, 1979.

The author is with the Satellite Communication Equipment Section, Electrical Communication Laboratories, Nippon Telegraph and Telephone Public Corporation, Yokosuka-shi, Kanagawa-Ken, 238-03 Japan.

This paper describes the structure, operation principle, theoretical analysis, design method, experimental results, and relations among ridge-shaped coupler and other slot-coupled couplers.

II. Structure and Operation Principle

The proposed ridge-shaped directional coupler structure is shown in Fig. 1. Two waveguides are coupled by one slot along the narrow wall. In this structure, the coupling region is a ridged waveguide in which TE_{10}, TE_{20}, and TE_{30} modes can propagate.

The fundamental operation of the ridge-shaped coupler can be described by the normal modes which satisfy the boundary conditions in the coupling region. Idealized field patterns for transverse electromagnetic field components E_y and H_x of the normal modes TE_{10}, TE_{20}, and TE_{30} are shown in Fig. 2. The other transverse field components, E_x and H_y, have much smaller amplitudes, so are not considered here.

Fig. 3 shows the 3-dB coupling process. If a main waveguide fundamental mode is incident into the coupling region from port ① of the bifurcated regions, TE_{10}, TE_{20}, and TE_{30} modes are simultaneously excited in phase in the coupling region, as shown in Fig.3(b). Judging from the continuous conditions of transverse electric and magnetic field components among the incident mode and these three modes, no reflection will occur. The excited TE_{10}, TE_{20}, and TE_{30} modes differ in phase velocity. Because of this difference, the phase relations among these three modes change along the waveguide, and these modes interfere with one another. The TE_{10} mode and the TE_{20} mode, however, do not interfere because of the field patterns, as shown in Figs.2(a) and (b).

The TE_{20} mode is practically unaffected by the coupling slot, since it has near-zero electric field in the slot. On the other hand, TE_{10} and TE_{30} modes are affected by the coupling slot. However, if the difference phase shift between TE_{10} and TE_{30} modes is 2π, the superposed electric field for these two modes is also near-zero in the coupling slot and unaffected by the slot.

From the above consideration, the ridge-shaped coupler nonreflecting condition can be expressed as

$$(\beta_{10}-\beta_{30})\cdot L=2\pi \tag{1}$$

0018-9480/80/0300-0239$00.75

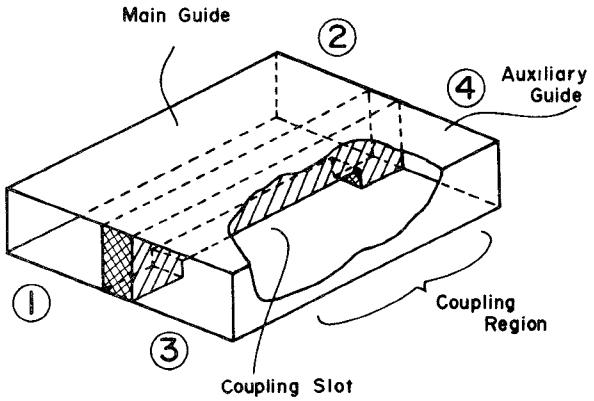

Fig. 1. Ridge-shaped directional coupler cutaway view.

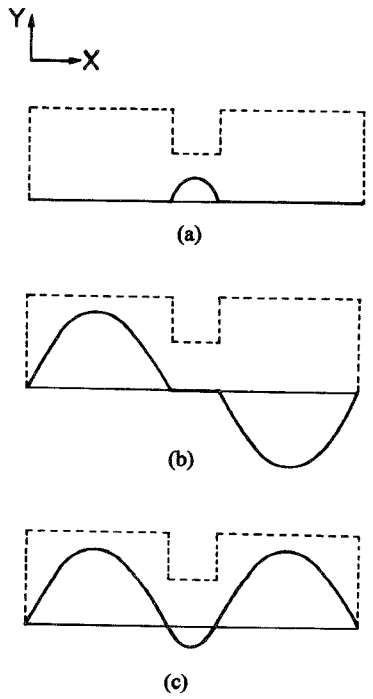

Fig. 2. Idealized field patterns in the coupling region. (a) TE_{10}. (b) TE_{20}. (c) TE_{30}.

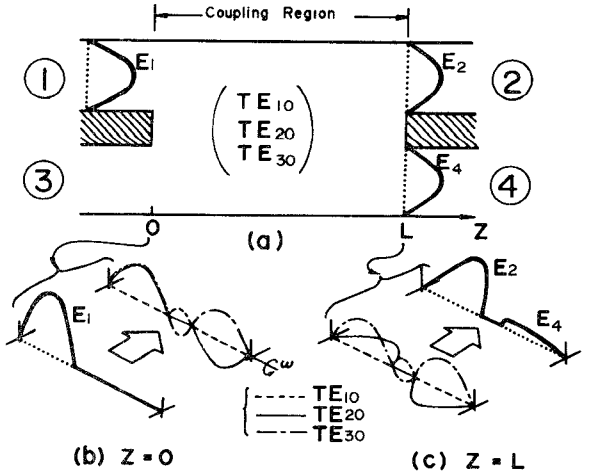

Fig. 3. 3-dB coupling process.

where

β_{10} TE_{10} mode propagation constant in the coupling region

β_{30} TE_{30} mode propagation constant in the coupling region

L coupling slot length.

The power transfer ratio is determined by TE_{20} and TE_{30} modes superposition. Therefore, 3-dB coupling condition can be expressed as

$$(\beta_{20}-\beta_{30})\cdot L=\pi/2 \tag{2}$$

where β_{20} is the TE_{20} mode propagation constant in the coupling region.

Fig. 3(c) shows 3-dB coupling at the end of the coupling region.

Incident wave E_1 for port ① and outgoing waves E_2 and E_4 for ports ② and ④ are expressed in the following relationship,

$$E_2=\frac{1}{2}(\exp(-j\beta_{20}L)+\exp(-j\beta_{30}L))E_1 \tag{3}$$

$$E_4=\frac{1}{2}(-\exp(-j\beta_{20}L)+\exp(-j\beta_{30}L))E_1. \tag{4}$$

Output powers P_2 and P_4 are derived from (3) and (4),

$$P_2=\frac{P_0}{2}(1+\cos(\beta_{20}-\beta_{30})\cdot L) \tag{5}$$

$$P_4=\frac{P_0}{2}(1-\cos(\beta_{20}-\beta_{30})\cdot L) \tag{6}$$

where P_0 is the input power.

The ratio of resultant waves in the two guides is

$$\frac{E_2}{E_4}=\frac{1}{j}\cot\left(\frac{(\beta_{20}-\beta_{30})\cdot L}{2}\right) \tag{7}$$

which indicates that the E_2 phase at the same cross section will lag that of E_4 by 90°, independently of the degree of power transfer. Furthermore, if a reference phase is chosen to be that phase of E_2 when there is zero coupling to the auxiliary guide, the E_2 phase will lead the reference phase by

$$\frac{(\beta_{20}-\beta_{30})\cdot L}{2}\text{ radian}$$

as the power transfer degree is increased. Amplitude and phase variations due to the coupling are shown in Fig. 4.

In the above description, evanescent higher order modes are not considered, since they have much smaller amplitudes than TE_{10}, TE_{20}, and TE_{30} modes.

III. Ridge-Shaped Coupler Design

This section deals with the case of designing the 3-dB coupler which satisfies conditions (1) and (2). The waveguide size discussed herein is 13×6.5 mm, which is almost the same size as the WRI-180 (12.954×6.477 mm).

A. TE_{10}, TE_{20}, and TE_{30} Modes Phase Constant

The cross-sectional shape of the coupling region in a ridge-shaped coupler is the same as the single ridged

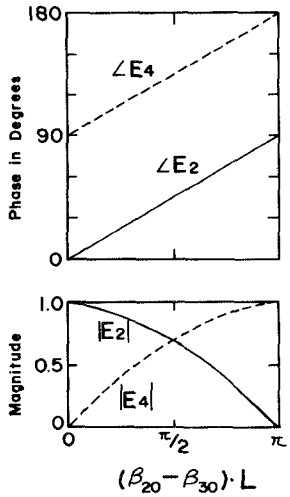

Fig. 4. Wave amplitude and phase factors versus $(\beta_{20}-\beta_{30})L$.

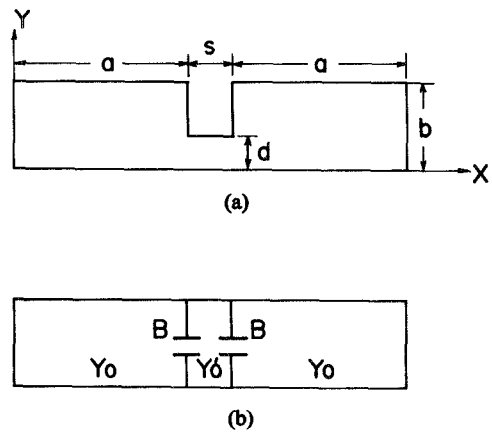

Fig. 5. Coupling region theoretical model and its equivalent circuit. (a) Single-ridge model. (b) Equivalent circuit.

waveguide, as shown in Fig. 5(a). Fig. 5(b) shows the equivalent circuit representation of Fig. 5(a).

Characteristic equations to determine the phase constants of the normal modes in the coupling region are determined by the transverse resonance method [4], as follows:

for $TE_{2n-1,0}$ mode $(n=1, 2, 3, \cdots)$

$$\cot k_c a - \frac{b}{d}\tan\frac{k_c s}{2} - \frac{B}{Y_0} = 0 \tag{8}$$

for $TE_{2n,0}$ mode $(n=1, 2, 3, \cdots)$

$$\cot k_c a + \frac{b}{d}\cot\frac{k_c s}{2} - \frac{B}{Y_0} = 0 \tag{9}$$

$$\beta^2 = k_0^2 - k_c^2$$

$$k_0 = 2\pi f\sqrt{\epsilon_0 \mu_0}$$

where

- β normal mode phase constant in the coupling region
- k_c transverse direction phase constant at cutoff
- k_0 free space wave number
- μ_0 permeability of free space
- ϵ_0 permittivity of free space
- f frequency
- a width of one guide
- b height of one guide
- s coupling slot width
- d coupling slot height.

Characteristic admittances Y_0 and Y_0' are defined as

$$Y_0 = \frac{k_c}{2\pi f\mu_0}\frac{1}{b} \qquad Y_0' = \frac{k_c}{2\pi f\mu_0}\frac{1}{d}. \tag{10}$$

The value of the normalized susceptance term B/Y_0, which represents the effect of the step discontinuity, has been obtained by Marcuvitz [5], as follows:

$$\frac{B}{Y_0} = \frac{2k_c b}{\pi}\left[\ln\left(\frac{1-\alpha^2}{4\alpha}\right)\left(\frac{1+\alpha}{1-\alpha}\right)^{1/2(\alpha+1/\alpha)} + 2\frac{A+A'+2C}{AA'-C^2} + \left(\frac{k_c b}{4\pi}\right)^2\left(\frac{1-\alpha}{1+\alpha}\right)^{4\alpha}\left(\frac{5\alpha^2-1}{1-\alpha^2}+\frac{4}{3}\frac{\alpha^2 C}{A}\right)^2\right] \tag{11}$$

where

$$A = \left(\frac{1+\alpha}{1-\alpha}\right)^{2\alpha}\frac{1+\sqrt{1-(k_c b/\pi)^2}}{1-\sqrt{1-(k_c b/\pi)^2}} - \frac{1+3\alpha^2}{1-\alpha^2}$$

$$A' = \left(\frac{1+\alpha}{1-\alpha}\right)^{2/\alpha}\frac{1+\sqrt{1-(k_c d/\pi)^2}}{1-\sqrt{1-(k_c b/\pi)^2}} + \frac{3+\alpha^2}{1-\alpha^2}$$

$$C = \left(\frac{4\alpha}{1-\alpha^2}\right)^2$$

$$\alpha = \frac{Y_0}{Y_0'} = \frac{d}{b}.$$

In order to investigate the normal modes which exist in the coupling region, the relations among β, d, and f, and among β, s, and f are shown in Fig. 6 and Fig. 7, respectively.

Slot width s is 4 mm in Fig. 6 and slot height d is 1.5 mm in Fig. 7. Since the operation of the ridge-shaped coupler is based on the interference among TE_{10}, TE_{20}, and TE_{30} modes, as described in Section II, higher order modes (TE_{n0}; $n \geqslant 4$) are useless and may cause resonances in the coupling slot. Therefore, it is necessary to design so that these higher order modes cannot propagate in the coupling region.

From Fig. 6, it is found that, as coupling slot height decreases, TE_{10} mode phase constant approaches free space wave number k_0 and TE_{20} and TE_{30} modes phase constants degenerate to that of the dominant mode of the bifurcated waveguide. From Fig. 7, the TE_{40} mode can propagate in the coupling region above a certain frequency, as coupling slot width increases.

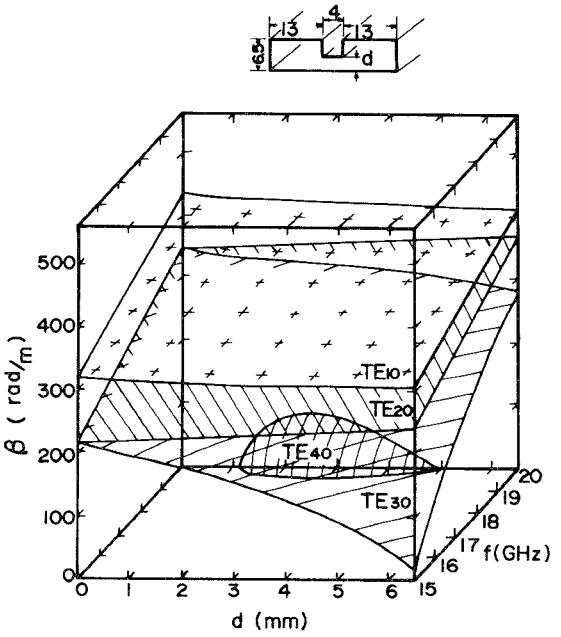

Fig. 6. Relations among phase constant β, coupling slot height d, and frequency f.

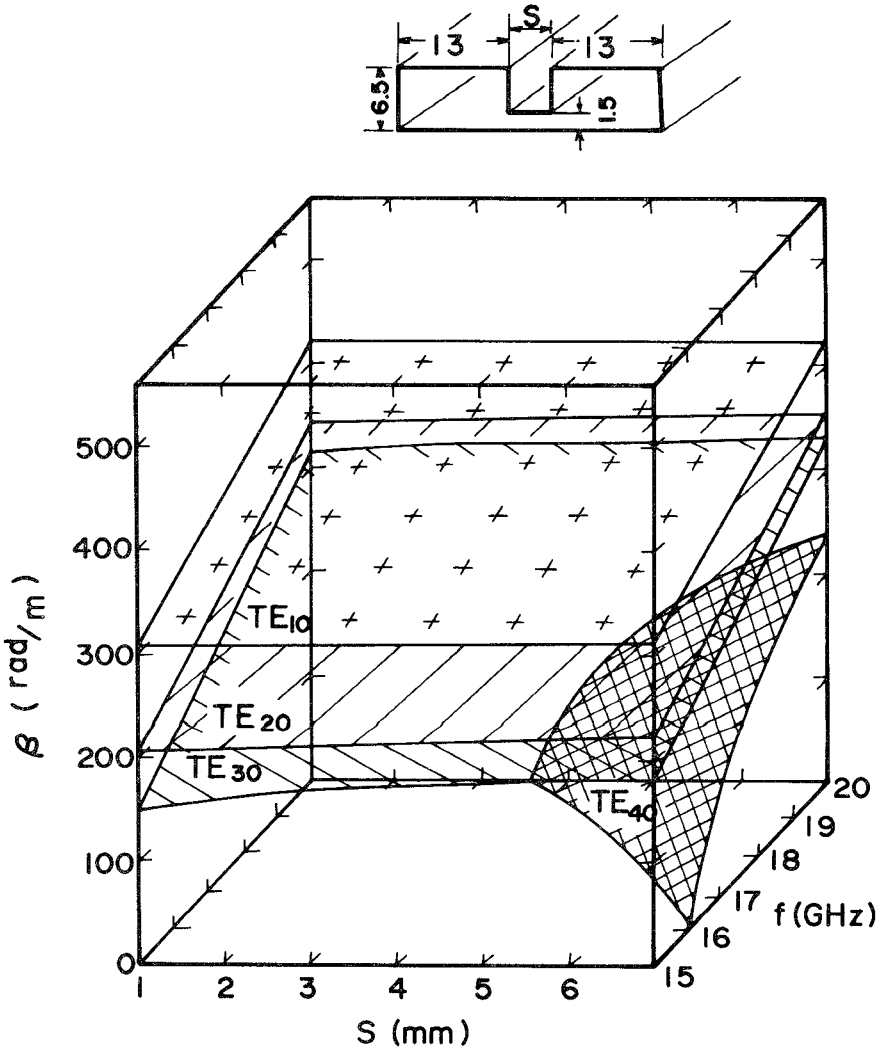

Fig. 7. Relations among phase constant β, coupling slot width s, and frequency f.

B. 20-GHz Band Ridge-Shaped Coupler

The requisite values for the coupler design are coupling slot width s, height d, and length L.

Let us consider $\beta_{10}-\beta_{30}$ and $\beta_{20}-\beta_{30}$ values, in order to examine the two conditions of (1) and (2). Variations in the above differential phase constants with s and d for several frequencies are shown in Fig. 8 and Fig. 9. In these figures, the broken line indicates that the TE_{40} mode can propagate in the coupling region. From Fig. 8, the $\beta_{10}-\beta_{30}$ and $\beta_{20}-\beta_{30}$ variations with s are small, so the ridge-shaped coupler can be fabricated without strict restriction for the dimensions between two coupled waveguides. In the following study, s is set up as 4.0 mm. From Fig. 9, the $\beta_{10}-\beta_{30}$ variation with d is small, which indicates that the nonreflecting condition can be satisfied with a suitable coupling slot length in spite of its height. On the other hand, the $\beta_{20}-\beta_{30}$ variation with d is proportional to the coupling slot height. Therefore, it is found that the ridge-shaped coupler can be used as a variable power divider by varying the coupling slot height.

The coupling length for 3-dB coupling is determined from Fig. 10. In Fig. 10, the chain line indicates the 3-dB coupling condition, while the solid line indicates the nonreflecting condition. Fig. 10 shows that these two conditions are satisfied simultaneously at $f=16.9$ GHz with $L=58$ mm, $d=1.4$ mm.

The couplings for ports ② and ④ from port ① are given by

$$C_{1-2}[\mathrm{dB}] = -10\log\left[\frac{1+\cos(\beta_{20}-\beta_{30})\cdot L}{2}\right] \quad (12)$$

$$C_{1-4}[\mathrm{dB}] = -10\log\left[\frac{1-\cos(\beta_{20}-\beta_{30})\cdot L}{2}\right]. \quad (13)$$

C. Electric and Magnetic Field Patterns

It is important to compute the transverse electric and magnetic field patterns in the coupling region, in order to show them to be similar to the field patterns shown in Fig. 2. The field computation herein depends on the method given by Getsinger [6]. The approach of this method is to assume a TEM parallel-plate guide mode in the region above the ridge and to match its electric field component at the edge of the ridge to the electric field components of a TEM parallel-plate guide mode plus higher order cutoff TM modes propagating transversely in the large end sections.

The computed results of E_y and H_x along X axis are depicted in Fig. 11 on an arbitrary scale. TE_{20} and TE_{30} mode patterns are very similar to those in Figs. 2(b) and (c), respectively. On the other hand, the TE_{10} mode pattern reveals the same tendency as in Fig. 2(a), i.e., the field concentrates in the coupling region. However, the TE_{10} mode field also exists in the large end-sections. Therefore, it is considered that the TE_{10} mode will influence the coupling characteristics to some degree.

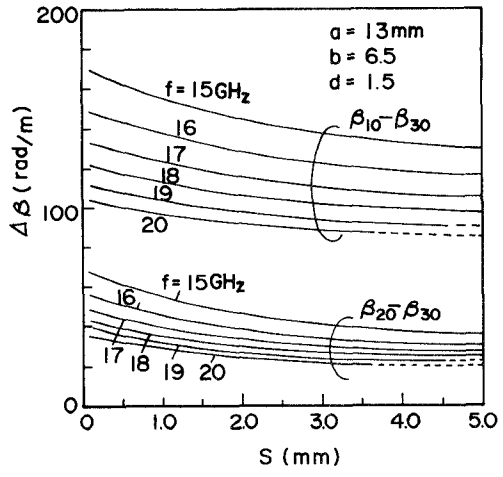

Fig. 8. Difference between phase constants ($\beta_{10}-\beta_{30}$ and $\beta_{20}-\beta_{30}$) versus coupling slot width s for several frequencies.

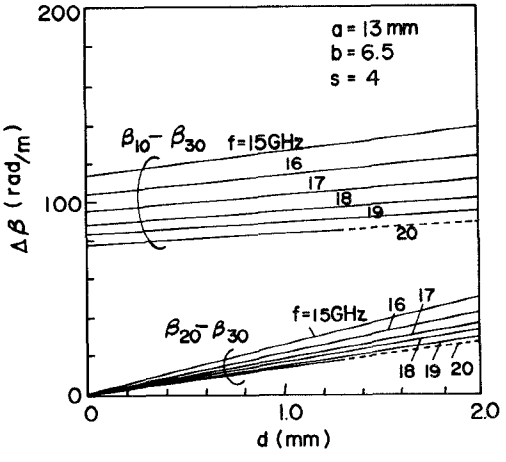

Fig. 9. Difference between phase constants ($\beta_{10}-\beta_{30}$ and $\beta_{20}-\beta_{30}$) versus coupling slot height d for several frequencies.

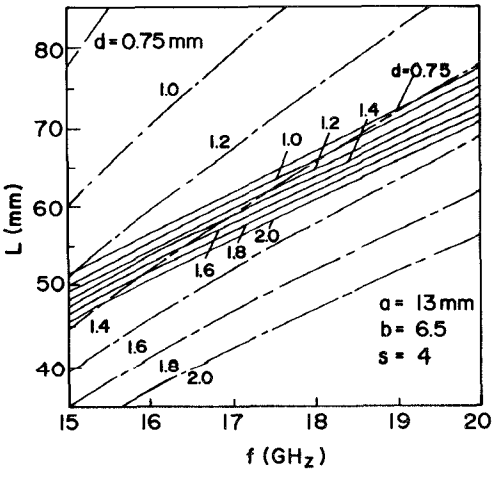

Fig. 10. Coupling length (L) versus frequency (f). ——nonreflection condition; ---3-dB coupling condition.

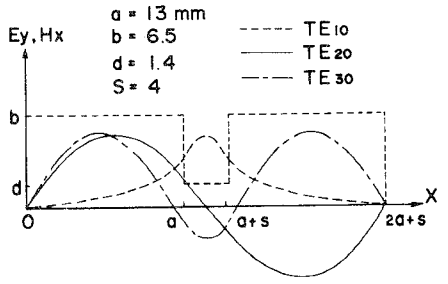

Fig. 11. Calculated field patterns along X axis.

IV. Experimental Results

A ridge-shaped directional coupler is shown in Fig. 12.

Fig. 13 shows the ridge-shaped coupler frequency characteristics. Theoretical and experimental results for the couplings are reasonably consistent with each other. Coupling equality is theoretically within ± 1.0 dB over the 16.0- to 19.0-GHz frequency range, whereas it is within ± 0.5 dB in the experiment. It can be considered that the difference between theoretical and experimental results is due to the TE_{10} mode influence in the coupling region. Insertion loss is less than 0.2 dB. Reflection loss ① –① and directivity ①–③ are both in excess of 30 dB. Peaks at 15.1 GHz and 19.8 GHz could be caused by the TE_{10} and TE_{30} mode resonances.

V. Relations to Other Slot-Coupled Hybrid Couplers

The upper part of Fig. 14 shows a cross-sectional view of slot coupled hybrid couplers, while the lower part of Fig. 14 shows the phase relationships in the above couplers [7]. Ridge-shaped hybrid couplers (single-ridge, double-ridge, and two-slot) are shown in Fig. 14.

It should be noted that main guide output signal E_2, in the short-slot, top-slot, and long-slot hybrids, lags the reference signal by 45°, while that in the ridge-shaped hybrid leads by 45°. Furthermore, auxiliary guide output signal E_4 lags main branch signal E_2 by 90° in the short-slot hybrid, but leads by 90° in the ridge-shaped, top-slot, and long-slot hybrids.

Several ridge-shaped directional coupler configurations are shown in Fig. 15. The coupling slot is able to be located in any portion of the narrow wall, as shown in Fig. 15(a). Furthermore, two coupling waveguides can be set up as shown in Figs. 15(b) and (c).

VI. Conclusion

A new directional coupler, whose operation principle is based on the interference among TE_{10}, TE_{20}, and TE_{30} modes, has been proposed and constructed in the 20-GHz band. Considering the good correspondence between theoretical calculation and experimental results, the design method presented here is reasonable and usable.

The ridge-shaped directional coupler is longer than the short-slot coupler and the bandwidth is about the same as the short-slot coupler when compared on the basis of

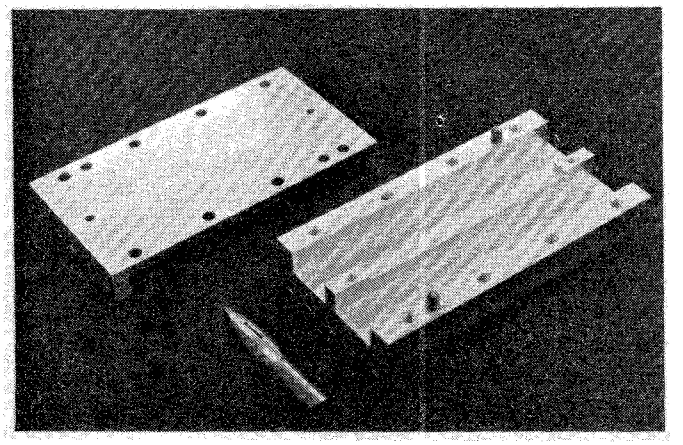

Fig. 12. Ridge-shaped directional coupler.

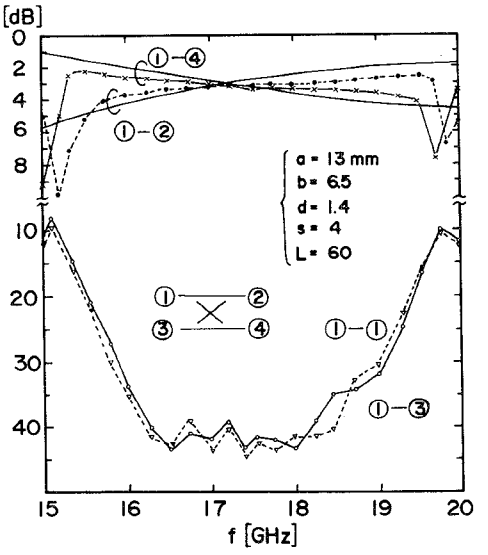

Fig. 13. Ridge-shaped coupler frequency characteristics. ——theory; ●, x, ○, △ experimental results.

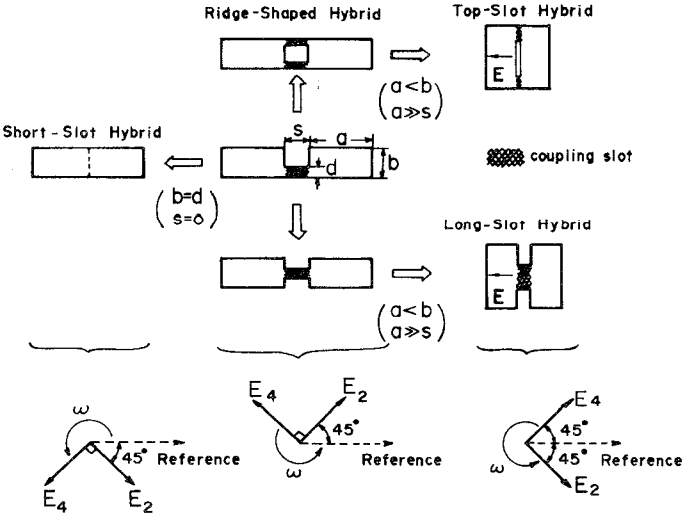

Fig. 14. Relations among ridge-shaped hybrid coupler and other slot coupled hybrid couplers.

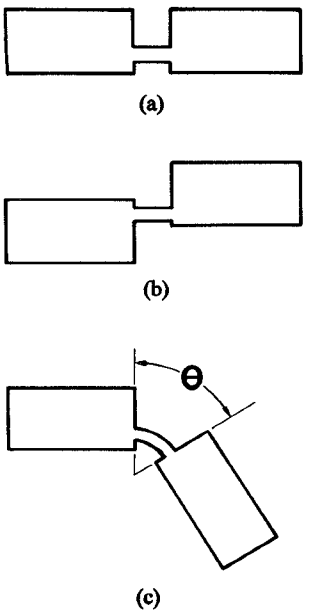

Fig. 15. Several ridge-shaped directional coupler configurations.

identical specification. But, the ridge-shaped coupler, which has many features as stated in the introduction, could be adaptable to microwave and millimeterwave devices.

The operation principle, based on interference among three normal modes, is applicable to the coupling between dielectric waveguides, so will have impact on optical integrated circuits.

Acknowledgment

The author wishes to thank Dr. T. Okajima, M. Kudo, T. Yoshikawa, and M. Kawai for their constant encouragement, and Dr. I. Ohtomo for his valuable discussion.

References

[1] H. J. Riblet, "The short-slot hybrid junction," *Proc. IRE,* vol. 40, p. 180, Feb. 1952.
[2] K. Tomiyasu and S. B. Cohn, "The Transvar directional coupler," *Proc. IRE*, vol. 41, p. 922, July 1953.
[3] R. Levy, "Directional couplers," in *Advances in Microwaves*, vol. 1, L. Young, Ed., New York: Academic Press, 1966.
[4] S. Hopfer, "The design of ridge waveguides," *IRE Trans. Microwave Theory Tech.*, vol. MTT-3, p. 20, Oct. 1955.
[5] N. Marcuvitz, *Waveguide Handbook*, New York: McGraw-Hill, 1951, ch. 5, p. 307.
[6] W. J. Getsinger, "Ridge waveguide field description and application to directional couplers," *IRE Trans. Microwave Theory Tech.*, vol. MTT-10, p. 41, Jan. 1962.
[7] H. E. Schrank and C. H. Grauling, Jr, "Phase relationships in short-slot hybrid couplers," *Proc. IRE,* vol. 47, p. 2017, Nov. 1959.